R2Co3-xSix (R = Pr, Nd, Sm, Gd) and R2Ni3-xSix (R = Gd-Er), new series of La2Ni3-type phases

Tadhg Mahon, Etienne Gaudin, Baptiste Vignolle, Géraldine Ballon, Bernard Chevalier, Sophie Tencé

$R_2Co_{3-x}Si_x$ (R = Pr, Nd, Sm, Gd) and $R_2Ni_{3-x}Si_x$ (R = Gd-Er), new series of La_2Ni_3-type phases

Tadhg Mahon[1, 2], Etienne Gaudin[1, 2, *], Baptiste Vignolle[1, 2, 3], Géraldine Ballon[3], Bernard Chevalier[1, 2], Sophie Tencé[1, 2,*]

[1] CNRS, ICMCB, UPR 9048, F-33600 Pessac, France

[2] Univ. Bordeaux, ICMCB, UPR 9048, F-33600 Pessac, France

[3] Laboratoire National des Champs Magnétiques Intenses (CNRS, INSA, UJF, UPS), 31400 Toulouse, France

[*]Corresponding authors, E-mail: etienne.gaudin@u-bordeaux.fr; sophie.tence@icmcb.cnrs.fr

Abstract

In this study, we have expanded our previous work on the $Gd_2(Co_{3-x}Si_x)$ system to form the family of $R_2(T_{3-x}Si_x)$ compounds with a wide range of the rare earth metals (Pr, Nd, Sm, Gd, Tb, Dy, Ho and Er) by variation of the composition and, where necessary, the transition element (Co and Ni). We report the crystallographic and the magnetic properties of this La_2Ni_3-type series. The $R_2Co_{3-x}Si_x$ compounds with R= Pr, Nd, Sm and Gd, undergo ferro- or ferrimagnetic transitions at T_C ranging from 64 K (Nd) to 338 K (Gd) and the $R_2Ni_{3-x}Si_x$ phases with R = Gd-Er display ferromagnetic order below T_C from 96 K (Gd) to 7 K (Er).

Keywords: Intermetallic, La_2Ni_3-type, Magnetic properties, Magnetocaloric

1. Introduction

Since the discovery of the giant magnetocaloric effect (MCE) by Pecharsky and Gschneidner in 1997 [1], the magnetocaloric effect has seen growing interest, in particular due to its possible applications in energy efficient refrigeration[2–4]. As the search for more energy efficient technologies gains popularity worldwide, the number of magnetocaloric materials (MCMs) being developed has only continued to grow [4–8] and a number of detailed review articles have been written on the effect and the types of materials that have been discovered [9,10]. Magnetocaloric materials which exhibit a second order ferromagnetic transition around the target application temperature are of great interest due to the easily reversible transition with little to no hysteresis, and the speed of the purely magnetic transition. To this end, significant work has been focused on the Gd-Co-Si system due to the high number of ferromagnetic phases with high transition temperatures that can be found therein [11–15]. During our study of this ternary system a new pseudo binary phase with the general formula $Gd_2(Co_{3-x}Si_x)$ has been discovered and its structural and magnetic properties investigated [11]. The phases with $0.29 < x < 0.50$ crystallize in the orthorhombic La_2Ni_3-type structure (*Cmce* space group) with unit cell parameters a = 5.3833(4) Å, b = 9.5535(6) Å, and c = 7.1233(5) Å for x = 0.47 and have a tuneable Curie temperature around room temperature

that is dependent on the Si concentration. Its crystal structure consists of a three dimensional network of Gd-atoms with puckered two dimensional Co/Si layers aligned along the *b*-axis. Following this discovery, Morozkin et al. [16] have stabilized the La_2Ni_3-type $R_2Ni_{2.5}Si_{0.5}$ (*R* = Dy, Ho) phases. In our work the structure has been stabilized for the majority of the other rare earth elements (Pr, Nd, Sm, Tb, Dy, Ho and Er) by varying the initial composition, annealing temperature, and where necessary, the transition element. This sequence, as well as its structural and magnetic properties, is subsequently presented here. A partial investigation of the $Gd_2Ni_{3-x}Si_x$ solid solution and the details of this work are also presented here.

2. Experimental

Samples were prepared by melting stoichiometric amounts of the pure elements (99.99 wt.% metal basis, supplied by STREM chemicals) in an arc furnace under an argon atmosphere. Initial samples were all made with the composition $R_2T_{2.5}Si_{0.5}$ (*R* = Ce, Pr, Nd, Sm, Gd, Tb, Dy, Ho, Er, *T* = Co, Ni). Following determination of phase composition by electron microprobe analysis new samples were made to reflect the actual composition of the phases in the samples: $Pr_2Co_{2.8}Si_{0.2}$, $Nd_2Co_{2.7}Si_{0.3}$, $Sm_2Co_{2.6}Si_{0.4}$, $Gd_2Co_{2.51}Si_{0.49}$, $Gd_2Ni_{3-x}Si_x$ ($0.35 \leq x \leq 0.6$) and $R_2Ni_{2.6}Si_{0.4}$ (*R* = Tb, Dy, Ho and Er). The samples were melted 3 times, turning in between each melting to improve homogeneity. In the case of the Pr and Nd samples 1-2 wt% extra rare earth element was added to account for mass loss due to volatility. Due to the high volatility of Sm, samples containing Sm were first melted three times in an induction furnace with a standard water cooled Cu crucible before melting a further three times in an arc furnace as with the other systems. 10 wt.% Sm was also added to account for mass loss during the synthesis. Levitation of the sample and cooling of the crucible prevented reaction with the copper crucible. For the heavy rare earth elements, weight losses were generally below 1% by mass. Annealing was carried out by sealing the samples in evacuated quartz ampoules and placing in a furnace at temperature ranging between 673 and 1073 K for four to twelve weeks. The annealing temperature was optimized for each sample and is given in table 1.

Routine x-ray powder diffraction (XRPD) was performed with the use of a Philips 1050-diffractometer (Cu-K_α radiation) for the structural characterization and phase identification of the as-cast and annealed samples. X-ray powder data for Rietveld analysis were collected at room temperature using a PANalytical X'pert Pro diffractometer working with the Cu-$K\alpha_1$ radiation (1.54051 Å) in the range $10 \leq 2\theta \leq 130°$ and a step size of 0.008°. Rietveld refinement and full pattern matchings were carried out using the Fullprof program package [17].

Magnetization measurements were performed using a superconducting quantum interference device (SQUID) magnetometer (Quantum Design MPMS-XL) in the temperature range 2 - 300 K and in fields up to 7 T. Susceptibility measurements were measured after Zero Field Cooling (ZFC) and Field Cooling (FC). High-field magnetization measurements were performed at the LNCMI in Toulouse using the compensated coil technique in a ^{4}He cryostat. The 14 MJ capacitor bank of the LNCMI was used to generate the pulsed field with a maximal

field strength of 56 T and a typical rise and fall time of 30 ms and 120 ms, respectively. The rising and falling part of the measurements show a good agreement, thus excluding any heating due to eddy currents. Various maximum field strengths (14T, 28T, 42T and 56T) have been used to ensure a good accuracy and reliability of the data.

Heat capacity was determined with a standard relaxation method using a Quantum Design PPMS device. Samples of approximately 10 mg were glued to the sample holder using Apiezon N-grease and the heat capacity of the sample holder and grease was measured just before the sample was studied.

Both the composition and the homogeneity of the as-cast and annealed samples were checked by microprobe analysis using a Cameca SX-100 instrument. The analysis by EDX (Energy Dispersive X-ray) was performed on the basis of intensity measurements of Gd-Lα_1, Co-Kα_1, Ni-Kα_1 and Si-Kα_1 x-ray emission lines, which were compared with internal standards of those elements within the instrument.

3. Results

3.1. Crystal structure and chemical composition

3.1.1. $R_2Co_{3-x}Si_x$

Annealing

The $R_2Co_{3-x}Si_x$ compounds (R = Ce, Pr, Nd, Sm and Gd) were annealed at various temperatures between 673 and 1073 K for several weeks. It was found through XRPD and microprobe analysis that for R = Ce the phase is not present either before or after annealing regardless of Si content (attempts were made for x = 0.4, 0.5 and 0.6) or annealing temperature. For R = Pr, Nd and Sm, the $R_2Co_{3-x}Si_x$ phase is not present before annealing and temperatures in excess of 823 K stabilize the RCo_2 instead of the $R_2Co_{3-x}Si_x$ phase. Thus, due to the low annealing temperatures required, at least two months of annealing were needed to attain good quality samples with the best samples being seen after three months of annealing. The only exception to this is the R = Gd case. Here the target phase was the major phase even after annealing at 1073 K for one month. The duration and annealing temperature are given for each sample in table 1. For the light rare earth elements (R = Pr, Nd and Sm), attempts to form the La_2Ni_3-type phase with T = Ni were unsuccessful.

Microstructural observations

The microprobe measurements confirm that the target phase is not obtained in the as-cast samples for R = Pr, Nd and Sm (*not shown here*). However, after annealing at 823 K for two to three months, the target phase was present, as visible for example in the back scattered electron (BSE) images of the annealed $R_2Co_{3-x}Si_x$ (R = Gd and Sm) samples (figure 1). We observe $R_2Co_{3-x}Si_x$ as the major phase with only small quantities of secondary phases spread homogeneously throughout the sample. The only exception to this is the $Gd_2Co_{3-x}Si_x$ system where the target phase crystallizes in small amounts from the melt on cooling which

confirms the previous results [11]. The EDX data for all the $R_2Co_{3-x}Si_x$ systems show only slight deviations between the nominal and measured compositions (table 1) with the exception of the *R* = Sm. For this sample the nominal x = 0.4 produces an effective x = 0.25. It was also observed that slightly varying the nominal composition changes the nature of the secondary phases and their relative quantities. In general, higher Si contents were found to stabilize the *RT*Si phase while lower concentrations stabilized the RT_2 phase with some small Si substitution (5-6 at%) on the transition element site as indicated in figure 1. It has already been documented that the annealing temperature can influence the final Si concentration in the main phase $Gd_2Co_{3-x}Si_x$ [11]. However, due to the long annealing times for all the Co samples (except *R* = Gd) the effect of annealing temperature was not investigated further here.

X-ray Powder Diffraction

XRPD measurements reveal that the $R_2Co_{3-x}Si_x$ samples (*R* = Pr, Nd or Sm) annealed above 823 K contain almost entirely RCo_2 with small quantities of *R*CoSi and $R_2Co_{3-x}Si_x$ as minor secondary phases. Only for the samples annealed at 823 K and below are the target $R_2Co_{3-x}Si_x$ phases present. The XRPD shows RCo_2, *R*CoSi and RCo_5 present as secondary phases (see figure 2 as example for *R* = Nd), in agreement with the microstructures observed in the microprobe images described in figure 1. $Gd_2Co_{3-x}Si_x$ is the only exception among the systems studied where the target phase was obtained for all investigated annealing temperatures. It was found to exhibit an increase in the Si content with increasing annealing temperature as explored in our previous publication on the $Gd_2Co_{3-x}Si_x$ system [11]. A summary of the unit cell parameters and annealing temperatures for all rare-earths is presented in table 1 and the unit cell parameters are plotted against rare earth radius in figure 3. The *b* and *c* parameters decrease with decreasing rare earth element radius (Pr → Gd) while the *a* parameter increases with an overall decrease in the unit cell volume. Increasing the silicon content as the rare earth radius decreases seems to improve the purity of the samples, (with the highest quality $Pr_2Co_{3-x}Si_x$ phase being observed for x = 0.2 while the Sm analogue was most pure for x = 0.4). As noted, the x = 0.4 nominal composition for $Sm_2Co_{3-x}Si_x$ produces an actual composition 0.25. Despite this difference, the XRPD pattern contained lower amounts of secondary phases for x = 0.4 than x = 0.3. This likely arises from the destabilization of the $SmCo_2$ phase through the shift in the composition.

Structural characterization

Figure 2 shows the results of Rietveld refinement on the $Nd_2Co_{2.7}Si_{0.3}$ sample after 3 months of annealing at 823 K and the main parameters of this refinement are summarized in table 2. The $Nd_2Co_{2.7}Si_{0.3}$ phase is present as the major phase with only small quantities of NdCoSi, $NdCo_5$ and $NdCo_2$ (3.60(7), 1.21(5) and 4.02(6) wt.% respectively) as secondary phases. $Nd_2Co_{2.7}Si_{0.3}$ crystallizes in the La_2Ni_3-type structure[18] previously described for $Gd_2Co_{3-x}Si_x$ [11]. The structural refinement indicates that Si substitution only occupies the Co2 (8*e*) site. Attempts to include Si substitution on the Co1 (4*a*) site only led to divergence in the refinement. This is different to the $Gd_2Co_{3-x}Si_x$ system described in reference [11], where Si

substitution was found mainly to occur on the Co1 site with only a small amount of Si located on the Co2 site. The Nd-Nd distances ranging from 3.42 to 3.44 Å (table 3) are considerably smaller than the ones for Nd metal [19] where $d_{Nd\text{-}Nd}$ = 3.643 Å. These Nd-Nd distances fall on the small side of the observed values for ternary Nd-Co-Si compounds such as NdCoSi [20] ($d_{Nd\text{-}Nd}$ = 3.885-4.010 Å), $NdCo_2Si_2$ [21] ($d_{Nd\text{-}Nd}$ = 4.007 Å) and $Nd_6Co_{1.67}Si_3$ [13] ($d_{Nd\text{-}Nd}$ = 3.502-3.697 Å). Similarly the Nd-Co binary systems such as $NdCo_2$ [22], $NdCo_5$ [23] and Nd_2Co_{17} [24] show $d_{Nd\text{-}Nd}$ = 3.161 Å, 3.960 Å and 3.836 Å respectively. Thus, $Nd_2Co_{2.7}Si_{0.3}$ exhibits Nd-Nd distances that are generally shorter than those observed in other similar compounds that have been studied. Conversely, the Gd-Gd distances in the $Gd_2Co_{3-x}Si_x$ system tend to be more comparable to those in the Gd-Co binary and Gd-Co-Si ternary systems. The Co/Si sublattice forms a puckered kagome-type lattice of hexagons running through the channels in the Nd network and in these hexagonal Co/Si rings the shortest distances lie between the Co1 and Co2/Si sites with d = 2.431(4) Å. This value lies between the sum of two covalent Co radii ($2r_{Co}$ = 2.52 Å) and the sum of the covalent Co and Si radii ($r_{Si} + r_{Co}$ = 1.11 Å + 1.26 Å = 2.37 Å) [25] This would tend to imply a largely covalent character to the Co-Co and Co-Si bonding in the hexagonal rings of the Kagome-type sublattice.

3.1.2. $R_2Ni_{3-x}Si_x$

Annealing

Unlike the $R_2Co_{3-x}Si_x$ compounds, the $R_2Ni_{3-x}Si_x$ phase is present as the major phase in the as cast samples for *R* = Gd-Er. Attempts to anneal these compounds from 673 to 1073 K stabilized RNi_2 as the major phase with only a small proportion of $R_2Ni_{3-x}Si_x$ present as a secondary phase. Thus, for the purposes of this study, only the as-cast samples were investigated thereafter. No La_2Ni_3-type phases were found for rare earth elements heavier than Gd for *T* = Co. The $Gd_2T_{3-x}Si_x$ system is the only one to exist for both *T* = Co and Ni. For the *R* = Gd-Dy, when x = 0.6 it was found that as cast samples contained a secondary phase with the Mo_2NiB_2 structure that was present as the major phase in the annealed samples. This phase will be discussed in more detail in the section on the x-ray diffraction experiments on the $R_2Ni_{3-x}Si_x$ phases.

Microstructural observations

From the $R_2Ni_{2-x}Si_x$ (*R* = Gd and Dy) examples in figure 1, it can be seen that the Ni-based phases form directly as the majority phase on cooling of the melt, in stark contrast to the systems where *T* = Co. The electron microprobe analyses show, in general, RNi_2 and *R*NiSi as secondary phases with a small amount of residual Dy_2O_3 in the case of the Dy sample. The composition of the major phases, as given by the EDX analysis, is very close to the nominal composition (table 4). Further microprobe analyses on the annealed Ni systems confirm that annealing the samples at all investigated temperatures led to growth of the RNi_2 and *R*NiSi phases at the expense of the $R_2Ni_{3-x}Si_x$ phase.

The $Gd_2Ni_{3-x}Si_x$ system was investigated in more detail with a total composition range of $0.35 \leq x \leq 0.6$. EDX analysis evidences that the most homogeneous sample, shown in figure

1, is obtained for x ≈ 0.4. The nature of the secondary phases changes based on the Si content: low Si concentrations causes an increase in the $GdNi_2$ Laves phase while higher Si amounts favor the formation of GdNiSi as a secondary phase. But, varying the nominal silicon content also modifies the amount of Si in the major phase, as measured by EDX analysis. Indeed, the effective x was found to vary from 0.40 to 0.65. The two extremes of this solid solution are also summarized in table 4.

X-ray Powder Diffraction

The XRPD measurements on the $R_2Ni_{3-x}Si_x$ systems confirm the results of the microprobe analysis, namely: i) the presence of the target phase in the as cast samples with good purity and; ii) the stabilization of the RNi_2 binary over the $R_2Ni_{3-x}Si_x$ phase upon annealing for all samples and at all investigated annealing temperatures. Figure 4 displays the Rietveld refinement of the XRPD data for the $Gd_{2.0}Ni_{2.6}Si_{0.4}$ sample with the refined crystal structure of $Gd_2Ni_{2.64(1)}Si_{0.36(1)}$ in the inset (see below). The Bragg peaks indicate that the phase crystallizes well on cooling from the melt. The unit cell parameters of the $R_2Ni_{3-x}Si_x$ phases are summarized in table 4. For the Ni systems, *a* remains mostly constant with *b* and *c* very slightly decreasing with rare earth size (figure 3). The evolution of the unit cell parameters is clearly much more pronounced in the case of *T* = Co than *T* = Ni. The observed changes in the *b* and *c* parameters in the Ni systems indicate that the rare earth radius has a much larger effect on these two axes than on the *a* axis. From this, we can assume that the puckered kagome-like lattice of Co/Si atoms is the most important sublattice with respect to the *a* axis. The rare earth sublattice plays a role through its contact with the intercalated kagome-like sheets of Co/Si in the *b* parameter and through the short *R*-*R* contacts in the *c* direction.

It is noteworthy that the samples with a high Si content (x = 0.6) with *R* = Gd, Tb, and Dy show a coexistence of the $R_2T_{3-x}Si_x$ phase with the La_2Ni_3 structure type and another phase crystallizing in the Mo_2NiB_2 structure type. The unit cell parameters of this second phase correspond to the $R_2Ni_{2.35}Si_{0.65}$ materials that were previously described by Morozkin *et al.* [16]. This result confirms their study of $Dy_2Ni_{3-x}Si_x$ and $Dy_2Ni_{2.35}Si_{0.65}$ which shows that the stability of the Mo_2NiB_2-type versus the La_2Ni_3-type structure is dependent on the Si content. In our study, most of the samples were only studied with low Si-content (x ≤ 0.6), which explains the stabilization of the La_2Ni_3-type structure over the Mo_2NiB_2-type materials. The other $R_2T_{3-x}Si_x$ phases were not studied for x > 0.5 and thus the existence of the Mo_2NiB_2 phase cannot be confirmed for the other rare earth elements. It should be recalled that only a few binary phases with La_2Ni_3-type structure have been evidenced in the past ([11] and references therein) and that our materials thus present an interesting addition to this small collection.

Structural characterization

Rietveld refinement was carried out on the as cast sample with nominal composition $Gd_2Ni_{2.6}Si_{0.4}$. The results of this refinement can be seen in figure 4 and are summarized in table 5. The major phase is clearly the desired La_2Ni_3-type $Gd_2Ni_{3-x}Si_x$ with only small quantities of $GdNi_2$ as a secondary phase (1.5(2) wt. %). Si substitution occurs only on the Ni1 (4*a*) site.

Possible Si substitution on the Ni2 (8*e*) site was initially included in the refinement but this led to divergence and so its occupancy on this site was fixed to zero. Si substitution on the Ni1 (4*a*) site agrees well with the result observed for the $Gd_2Co_{3-x}Si_x$ system where the substitution also occurs principally on the 4*a* site. Interestingly, this result differs from that observed for the lighter rare earth elements where, as mentioned, Si substitution occurs on the 8*e* site. This may be due to the larger size of the light rare earths. The interatomic distances for $Gd_2Ni_{2.6}Si_{0.4}$ can be seen in table 6. The shortest Gd-Gd distances in this system are 3.33 to 3.45 Å which are smaller than the typically observed 3.574 to 3.636 Å for Gd metal [26], but resemble other compounds in the Gd-Ni-Si ternary phase diagram such as $Gd_6Ni_{1.67}Si_3$ [13] (d_{Gd-Gd} = 3.456 to 3.867 Å) and GdNiSi [27] (d_{Gd-Gd} = 3.497 to 3.596 Å). The shortest Ni-Ni and Ni-Si distance of 2.442 Å lies closer to the sum of two covalent Ni radii ($2r_{Ni}$ = 2.42 Å) than to the sum of the covalent radii of Ni and Si ($r_{Ni} + r_{Si}$ = 1.24 Å + 1.11 Å = 2.35 Å [25]). Considering the relative proportions of the two elements, it is unsurprising that the average bond distance would tend to be closer to that of the purely Ni case.

3.2. Magnetic measurements

3.2.1. $R_2Co_{3-x}Si_x$

Magnetization vs. temperature M(T) measurements were carried out at 0.05 T on $R_2Co_{3-x}Si_x$ samples. The results of these measurements can be seen in figure 5 and table 1. These compounds undergo ferromagnetic ordering at T_C = 64, 159 and 267 K for samples with nominal composition $Pr_2Co_{2.8}Si_{0.2}$, $Nd_2Co_{2.7}Si_{0.3}$ and $Sm_2Co_{2.6}Si_{0.4}$. As a reminder, $Gd_2Co_{3-x}Si_x$ orders ferrimagnetically due to the antiferromagnetic coupling between the Co moments and the heavy-lanthanide ones [11]. As with the pure rare earth elements, an increase in the Curie temperature of the $R_2Co_{3-x}Si_x$ systems is thus observed moving along the lanthanide block with a maximum at Gd since T_C = 280-338 K for $Gd_2Co_{3-x}Si_x$ with $0.3<x<0.5$ [11]. Besides the main transitions, the Pr, Nd and Sm samples exhibit a second anomaly at a lower temperature. In the case of $Pr_2Co_{2.8}Si_{0.2}$ and $Nd_2Co_{2.7}Si_{0.3}$ the small upturns at T = 40 and 100 K correspond well with the T_C values of $PrCo_2$ [28] and $NdCo_2$ [22]. Both of these phases were observed in small amounts in the XRPD patterns. For the $Sm_2Co_{2.6}Si_{0.4}$ sample it is unknown if the anomaly at 200 K is intrinsic to the main phase or if it in fact is due to the presence of $SmCo_{2-x}Si_x$ ($x \approx 0.18$) (T_C = 230 K for $SmCo_2$) [29]) evidenced in the microprobe and XRPD analysis of this sample. Burzo *et al.* [30] demonstrated that the substitution of Si onto the cobalt site for $GdCo_{2-x}Si_x$ can lower the T_C of the phase thus a similar phenomenon may be happening here with $SmCo_{2-x}Si_x$. The final possible explanation for this second transition is the phase observed in the microprobe analysis with composition $Sm_{49}Co_{41}Si_{10}$ which has not been documented before. As its magnetic properties are unknown, we cannot currently confirm if the transition at 200 K corresponds to this phase.

One of the most interesting systems is $Pr_2Co_{2.8}Si_{0.2}$. Figure 6 displays the ZFC and FC magnetization curves measured at 0.05 T, 2 T and 3 T as well as the inverse of the susceptibility at high temperatures and 2 T. The Pr compound follows a Curie-Weiss behavior

at high temperature with a paramagnetic Curie temperature, θ_P, of 90 K and an effective moment μ_{eff} = 7.2 μ_B f.u.$^{-1}$, *i.e*. 5.1 μ_B Pr^{-1} if only Pr is magnetic. For a Pr^{3+}, μ_{eff} is expected to be equal to 3.58 μ_B and thus the larger experimental value of μ_{eff} evidences that Co also carries a magnetic moment. The effective magnetic moment for Co is calculated to be 3.07 μ_B Co^{-1} ($\mu_{eff}^2 = 2.8\mu_{eff(Co)}^2 + 2\mu_{eff\ (Pr3+)}^2$). The fact that Co-atoms carry a magnetic moment has been previously evidenced by Gignoux *et al*. through neutron diffraction studies of the La_2Co_3 phase with μ_{Co} = 0.73 μ_B [31]. Therefore, one can assume the presence of magnetic interactions between the Pr and the Co sublattices. This explains the relatively high Curie temperatures of this material and more generally of the whole $R_2Co_{3-x}Si_x$ family. From the M(T) curves of $Pr_2Co_{2.8}Si_{0.2}$, it is clear that the Curie temperature has a significant magnetic field dependence, T_C increasing by almost 33 K (from 64 to 97 K) when moving the field from 0.05 T to 3 T. We also notice a strong irreversibility between the ZFC and the FC curve below T_C. This indicates strong magnetocrystalline anisotropy. Additionally, a number of jumps are observed in the M(H) curves presented in figure 7, revealing a complex magnetic behavior. At 110 K, the jump around 4.5 T clearly results from a paramagnetic to ferromagnetic state transition since at this temperature the compound is in its paramagnetic domain below 2 T as seen in the M(T) curves. At 150 K no field-induced ferromagnetic transition is visible up to 7 T. At lower temperatures the critical field H_c at the jump increases with decreasing temperature from 65 to 5 K. In this temperature range, the jump in the M(H) curve may be attributed to strong domain wall pinning in the ferromagnetic state.

To further investigate the magnetocrystalline anisotropy in the $Pr_2Co_{2.8}Si_{0.2}$ sample, magnetization hysteresis loops were performed on both powder and a piece of the polycrystalline sample (figure 8). The powder magnetization curve exhibits a higher value at 7 T and a much smaller coercive field than that of the piece since the powder grains are free to rotate with the field. These differences clearly reveal the strong magnetocrystalline anisotropy in $Pr_2Co_{2.8}Si_{0.2}$. The powder magnetization at 7 T of 6.03 μ_B f.u.$^{-1}$ results from the contribution of both Pr and Co sublattices which are expected to be coupled ferromagnetically. The piece sample exhibits extreme magnetic hysteresis consistent with a hard magnetic material. A remanent magnetization of 3.4 μ_B f.u.$^{-1}$ is observed with a coercive field of 6.6 T. This provides a calculated BH_{max} of 70 MG Oe (556 kJ m^{-3}) but due to the low ordering temperature this material is not interesting for permanent magnet uses.

Figure 9 (left) shows the inverse susceptibility of the $Nd_2Co_{2.7}Si_{0.3}$ sample, fitted using the Curie-Weiss law. Like the $Pr_2Co_{2.8}Si_{0.2}$ system, $Nd_2Co_{2.7}Si_{0.3}$ was also found to be a Curie-Weiss paramagnet. The θ_P = 143 K is close to the observed Curie temperature of 159 K and, the system exhibits an effective magnetic moment of 6.2 μ_B f.u.$^{-1}$. Like the Pr analogue, this is much larger than the expected value for R^{3+} ion (5.19 μ_B for 2 Nd^{3+} in the formula unit), indicating that the magnetism arises from more than just the Nd atoms. The Co atoms were found to have a calculated effective magnetic moment of 2.15 μ_B. Thus the Co sublattice is magnetically active, as in all of the investigated materials in the $R_2Co_{3-x}Si_x$ system (*R* = Pr and

Nd). Due to the high transition temperature of the Sm compound its own Curie-Weiss behavior could not be investigated.

3.2.2. $R_2Ni_{3-x}Si_x$

The M(T) curves for the $R_2Ni_{2.6}Si_{0.4}$ systems are shown in figure 10. They show sharp ferromagnetic transitions with T_C decreasing continually moving from Gd → Er as expected from the trends observed in the pure rare earth metals. The Curie temperatures observed are 96, 78, 46, 28, and 7 K for R = Gd, Tb, Dy, Ho and Er, respectively (summarized in table 2). The variation of the T_C with changing rare earth element corresponds with the trend in the de Gennes factors for each element as seen in the inset of figure 10. Small, additional transitions can be observed at 89 K in $Gd_2Ni_{2.6}Si_{0.4}$, 29 K in $Dy_2Ni_{2.6}Si_{0.4}$, 18 K in $Ho_2Ni_{2.6}Si_{0.4}$ and 20 K in $Er_2Ni_{2.6}Si_{0.4}$. These all correspond well with the reported values for the T_Cs of the RNi_2 phases [32]. Furthermore, the investigation of the $Gd_2Ni_{3-x}Si_x$ ($0.35 \leq x \leq 0.6$) reveals that the Si content has no effect on the T_C of the materials. This indicates that the Ni sublattice does not contribute to the magnetic properties of this material.

Figure 9 (right) plots the inverse susceptibility of $Gd_2Ni_{2.6}Si_{0.4}$ against temperature. The curve was fitted using a Curie-Weiss law between 130 and 360 K and good agreement was found. The θ_P of 104 K is close to the observed T_C of 96 K and the positive value suggests ferromagnetic interactions. The calculated effective moment of 8.16 μ_B Gd^{-1} is slightly higher than the theoretical value (7.94 μ_B) seen in Gd^{3+} systems. However, Gd-based intermetallics sometimes exhibit higher magnetic moments due to hybridization between 4*f* electrons and 5*d* conduction electrons [33]. This yields effective magnetic moments in excess of 7.94 μ_B [34,35] and is likely the cause of the high effective moment here.

3.2.3. High-field magnetization measurements

The previously documented magnetic properties of $Gd_2Co_{3-x}Si_x$ [11] illustrate that the T_C is tuneable between 280 and 338 K by varying x between 0.29 and 0.50. M(H) measurements at low temperatures for this solid solution showed that M_{sat} = 12.66 μ_B/f.u. at 4.5 T. As the saturated magnetization is expected to be at least equal to 14 μ_B/f.u. (7 μ_B/Gd) if only Gd atoms carry a magnetic moment, this provides strong evidence that the Co sublattice is magnetic, as in the other $R_2Co_{3-x}Si_x$ phases (*R* = La, Pr, Nd). Indeed, the lower than expected moment is likely due to anti-ferromagnetic coupling between the Co and Gd sublattices for an overall ferrimagnetic order. In order to investigate this, high field magnetization measurements were carried out on both $Gd_2Ni_{2.6}Si_{0.4}$ and $Gd_2Co_{2.52}Si_{0.48}$ at magnetic fields of up to 56 T the results of which can be seen in figure 11 where only the rising part of the pulse is displayed. From these high field measurements it can be seen that $Gd_2Ni_{2.6}Si_{0.4}$ becomes fully saturated around 10 T with μ_{sat} = 15.4 μ_B $f.u.^{-1}$ or 7.7 μ_B Gd^{-1}, slightly higher than the values expected for the free Gd^{3+} ion of 7.0 μ_B. As above-mentioned for the experimental effective moment, this excess of moment value is likely due to conduction electron contribution. The assumption of Ni atoms carrying spins is ruled out since the Curie temperature is low compared to that of the Co homologue and T_C is almost independent of

the Ni content unlike the T_C of the $Gd_2Co_{3-x}Si_x$ compounds. Moreover, either the magnetization value at high field would be lower than 14 μ_B/f.u. as for an expected antiferromagnetic coupling between Gd and Ni sublattices or a second increase of the magnetization would be seen before reaching μ_{sat} = 15.4 μ_B/f.u. resulting from the alignment process of both sublattices. Conversely, saturation of the magnetization of $Gd_2Co_{2.52}Si_{0.48}$ requires much higher fields and only produces μ_{sat}= 12.6 μ_B/f.u. Due to this value being significantly below 14 μ_B/f.u., it is logical to conclude that there is an anti-ferromagnetic coupling between the Gd and Co sublattices up to 56 T. Thus, we can assume that a higher critical field is required to align both sublattices along the magnetic field due to strong exchange coupling between Gd and Co sublattices.

3.2.4. Magnetocaloric effect.

The presence of pronounced ferromagnetic transitions in most of the $R_2T_{3-x}Si_x$ materials makes them promising candidates for potential magnetocaloric materials. The magnetocaloric effect (MCE) is notably quantified by the isothermal magnetic entropy change (ΔS_m). This can be indirectly calculated from measurements of magnetization against field using Maxwell's relationship below.

$$\Delta Sm = \int_0^H \left(\frac{\partial M}{\partial T}\right)_H dH$$

The MCE for the $Gd_2Co_{3-x}Si_x$ system was previously documented by Tencé *et al.* [11] and found to have a $\Delta S \approx 1.7$ J kg^{-1} K^{-1} in a field of 2 T at the Curie temperature (287 K). The isothermal magnetic entropy change was measured for the $Gd_2Ni_{2.6}Si_{0.4}$ system (figure 12) and found to be quite large by comparison with a $\Delta S \approx 5.1$ J kg^{-1} K^{-1} in a field of 2 T at the T_C (96 K) of the compound. The lower Curie temperature explains partly the strong difference between both values (a factor of 3). Besides the ferrimagnetic structure of the Co compound versus the ferromagnetic structure of the Ni compound likely plays a role in this difference. As the Si content of the $R_2Ni_{3-x}Si_x$ does not impact the transition temperature, it is not possible to use the composition to tune the T_C and induce an internal concentration gradient with a corresponding gradient in the T_C of the material as with the Co analogue. This could create a so called "table top MCE" which is a highly desirable phenomenon in practical magnetic refrigerants. It can also be seen from Figure 12 that the MCE is still reasonably high up to 15-20 K from the T_C meaning that this material can produce a considerable MCE over a temperature range of roughly 40 K. For comparison, the study of the magnetocaloric properties of the Mo_2NiB_2-type phase $Gd_2Ni_{2.35}Si_{0.65}$ by Morozkin et al. shows $\Delta S_m \approx 7$ J kg^{-1} K^{-1} in a field of 2 T at around 66 K [16]. This value is slightly higher but for a lower magnetic ordering temperature. As pointed by Tencé et al. [36] the magnetocaloric performance of Gd-based systems showing second-order transition is directly correlated to the amount of Gd and the magnetic ordering temperature.

4. Conclusion

The new pseudo-binary $R_2T_{3-x}Si_x$ phase has now been shown to exist for a wide range of the rare earth elements. For rare earth elements smaller than Gd the phase was only found to be stable with Ni and, conversely, for the rare earth elements larger than Gd the phase could only be stabilized with Co. Gd has been shown to form the phase with both Ni and Co. The magnetic properties of the cobalt sub-lattice mean that those systems' magnetic properties are far more susceptible to composition changes than the Ni analogues with the heavier rare earths which contain a non-magnetic Ni sub-lattice. Thus the T_Cs of these $R_2Co_{3-x}Si_x$ systems can potentially be tuned by varying the initial composition. It was found from high field measurements that the $Gd_2Co_{3-x}Si_x$ system exhibits ferrimagnetic behavior while the same system with Ni instead of Co is purely ferromagnetic. All systems exhibited some indications of solid solution behavior; however, outside of a small composition range the phase tends to contain large concentrations of secondary phases and the solid solution was only investigated in the $Gd_2Ni_{3-x}Si_x$ case for $0.35 \leq x \leq 0.6$. The MCE was measured for the $Gd_2Ni_{2.63(1)}Si_{0.37}$ compound and found to be equal to $\Delta S \approx 5.1$ J kg^{-1} K^{-1} in a field of 2 T at around 100 K.

Tables:

Table 1. Compositions, annealing temperatures (T_A) and durations, Curie temperatures (T_C), and unit cell parameters of the $R_2Co_{3-x}Si_x$ systems.

Nominal composition	**$Pr_{2.0}Co_{2.8}Si_{0.2}$**	**$Nd_{2.0}Co_{2.7}Si_{0.3}$**	**$Sm_{2.05}Co_{2.55}Si_{0.40}$**	**$Gd_{2.00}Co_{2.55}Si_{0.45}$**	**$Gd_{2.05}Co_{2.52}Si_{0.48}$**
Composition*	$Pr_{2.00(2)}Co_{2.85(2)}Si_{0.15(1)}$	$Nd_{1.95(12)}Co_{2.8(3)}Si_{0.30(9)}$	$Sm_{2.10(13)}Co_{2.65(11)}Si_{0.25(5)}$	$Gd_{2.00(10)}Co_{2.63(9)}Si_{0.37(5)}$	$Gd_{2.05(10)}Co_{2.50(9)}Si_{0.45(5)}$
T_A (K)	823	823	823	773	1073
Duration (days)	93	93	93	30	30
T_C (K)	64(2)	159(2)	267(2)	327(2)	284(2)
***a* (Å)**	4.9064(3)	4.99436(10)	5.3045(7)	5.3681(4)	5.3822(1)
***b* (Å)**	10.0826(5)	9.99176(13)	9.6625(1)	9.5610(6)	9.5503(2)
***c* (Å)**	7.6451(5)	7.54912(10)	7.2229(1)	7.1254(5)	7.1213(1)
V (Å^3)	378.20	376.72	370.21	365.68	366.05
Ref	*this work*	*this work*	*this work*	[11]	*this work*

*Determined from EDX analysis

Table 2. Atomic positions, isotropic Debye-Waller factor (B_{iso}) and occupancy for sample with nominal composition $Nd_2Co_{2.7}Si_{0.3}$ and refined composition $Nd_2Co_{2.58(4)}Si_{0.42(4)}$

Position	**Wyckoff**	**x**	**y**	**z**	**B_{iso}**	**Occupancy**
Co1	4*a*	0	0	0	0.4(2)	1
Co2	8*e*	0.25	0.089(1)	0.25	0.4(2)	0.79(2)
Si	8*e*	0.25	0.089(1)	0.25	0.2(2)	0.21(2)
Nd	8*f*	0	0.344(3)	0.095(3)	0.77(3)	1

Table 3. Interatomic distances in Å for nominal $Nd_2Co_{2.7}Si_{0.3}$

Nd	**Nd**	**3.42(2)**
	Nd	**3.43(4)**
	Nd	**3.44(3)**
	Co1	**3.030(16)**
	Co1	**3.43(2)**
	Co1	**3.51(3)**
	Co2/Si	**2.96(2)**
	Co2/Si	**2.99(3)**
	Co2/Si	**3.07(3)**
Co1	**Co2/Si**	**2.431(4)**
Co2/Si	**Co2/Si**	**2.4972(1)**

Table 4. Curie temperatures T_C and unit cell parameters of the as-cast $R_2Ni_{3-x}Si_x$ systems.

Nominal Composition	**$Gd_{2.0}Ni_{2.6}Si_{0.4}$**	**$Gd_{2.0}Ni_{2.4}Si_{0.6}$**	**$Tb_{2.0}Ni_{2.6}Si_{0.4}$**	**$Dy_{2.0}Ni_{2.6}Si_{0.4}$**	**$Ho_{2.0}Ni_{2.6}Si_{0.4}$**	**$Er_{2.0}Ni_{2.6}Si_{0.4}$**
Composition*	$Gd_{2.00(1)}Ni_{2.60(15)}Si_{0.40(6)}$	$Gd_{2.00(10)}Ni_{2.4(2)}Si_{0.65(1)}$	$Tb_{2.00(10)}Ni_{2.55(10)}Si_{0.45(10)}$	$Dy_{2.00(11)}Ni_{2.60(15)}Si_{0.40(9)}$	$Ho_{2.00(10)}Ni_{2.70(10)}Si_{0.30(10)}$	$Er_{2.00(15)}Ni_{2.70(10)}Si_{0.30(5)}$
T_C (K)	96(2)	96(2)	78(2)	46(2)	28(2)	7(2)
***a* (Å)**	5.26733(5)	5.2665(1)	5.2438(3)	5.2398(4)	5.2511(3)	5.2599(2)
***b* (Å)**	9.30192(7)	9.3082(1)	9.2331(4)	9.1880(6)	9.1657(4)	9.1477(4)
***c* (Å)**	7.40978(6)	7.4110(2)	7.3640(5)	7.3453(5)	7.3011(5)	7.2464(3)
V (Å^3)	363.05	363.30	356.54	353.63	349.48	348.67

*Determined from EDX analysis

Table 5. Atomic positions, isotropic Debye-Waller factor (B_{iso}) and occupancies for the sample with nominal composition $Gd_2Ni_{2.6}Si_{0.4}$ and refined composition $Gd_2Ni_{2.64(1)}Si_{0.36(1)}$

Position	Wyckoff	x	y	z	B_{iso}	Occupancy
Ni1	4*a*	0	0	0	0.493(13)	0.64(1)
Si	4*a*	0	0	0	0.493(13)	0.36(1)
Ni2	8*e*	0.25	0.096(2)	0.25	0.493(13)	1
Gd	8*f*	0	0.340(4)	0.100(2)	0.493(13)	1

All B_{iso} had to be constrained to be the same as the Gd one to avoid negative values

Table 6. Interatomic distances for $Gd_2Ni_{2.64(1)}Si_{0.36}$ in Å.

Gd	**Gd**	**3.33(5)**
	Gd	**3.446(14)**
	Gd	**3.45(3)**
	Ni2	**2.94(3)**
	Ni2	**2.85(3)**
	Ni2	**2.969(15)**
	Ni1/Si1	**3.12(2)**
	Ni1/Si1	**3.25(4)**
	Ni1/Si1	**3.32(2)**
Ni1/Si1	**Ni2**	**2.442(7)**
Ni2	**Ni2**	**2.6337(1)**

Figures:

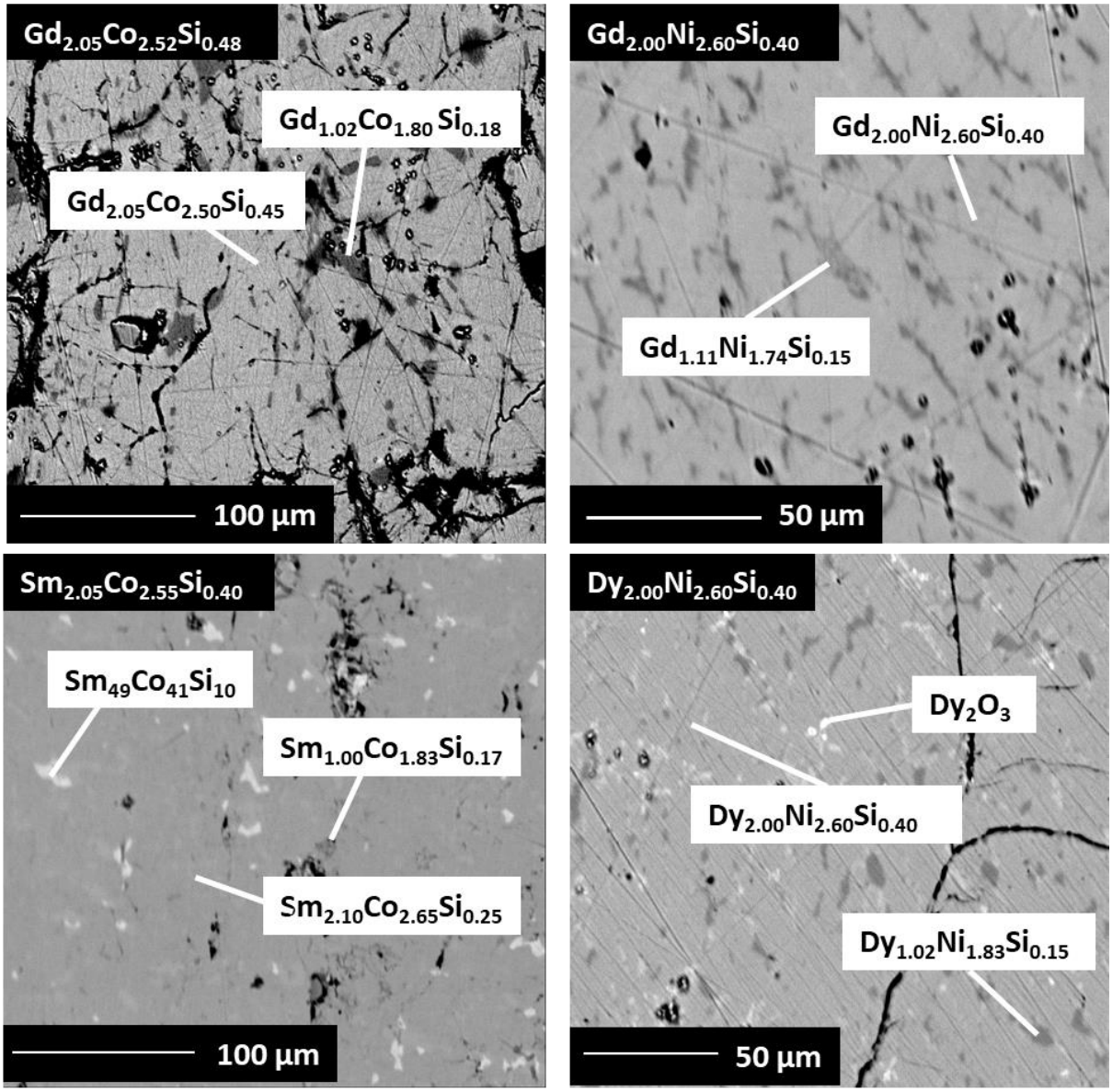

Figure 1. Back scattered electron images from the electron microprobe analysis of the $R_2Co_{3-x}Si_x$ (R = Gd and Sm) and $R_2Ni_{3-x}Si_x$ systems (R = Gd and Dy). Annealing conditions for $R_2Co_{3-x}Si_x$ samples are given in Table 1. The $R_2Ni_{3-x}Si_x$ samples are shown in the as-cast state. The nominal composition is given in the black rectangle and the compositions deduced from microprobe analysis in white rectangles.

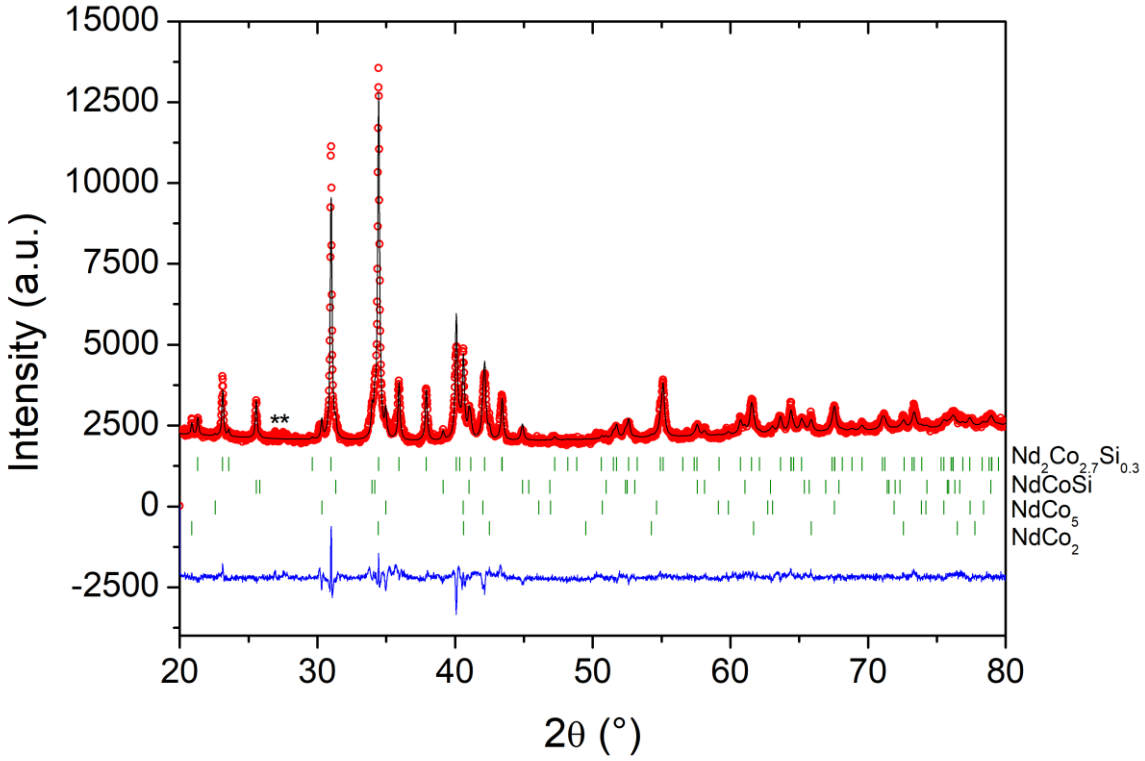

Figure 2. (Color online) Rietveld refinement of the crystal structure using the X-ray powder diffraction pattern for the $Nd_2Co_{2.7}Si_{0.3}$ system after annealing at 823 K for 2 months. The * symbols indicate a small amount of the Nd_2O_3 impurity phase that was not taken account in the refinement.

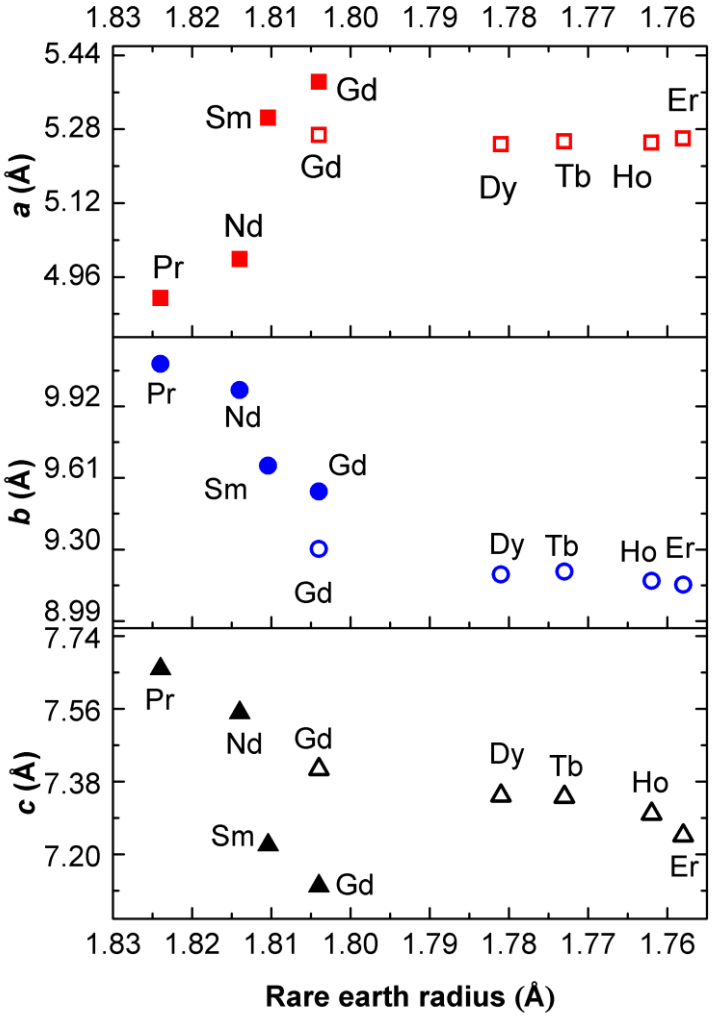

Figure 3. Unit cell parameters for each of the $R_2T_{3-x}Si_x$ phases, as summarized in Table 1 and 4, plotted against the rare earth radii [37]**. The filled points represent the systems where *T* = Co and the hollow points the systems where *T* = Ni. For the sake of clarity the points for *R* = Sm and Er correspond to a slightly shifted rare earth radius.**

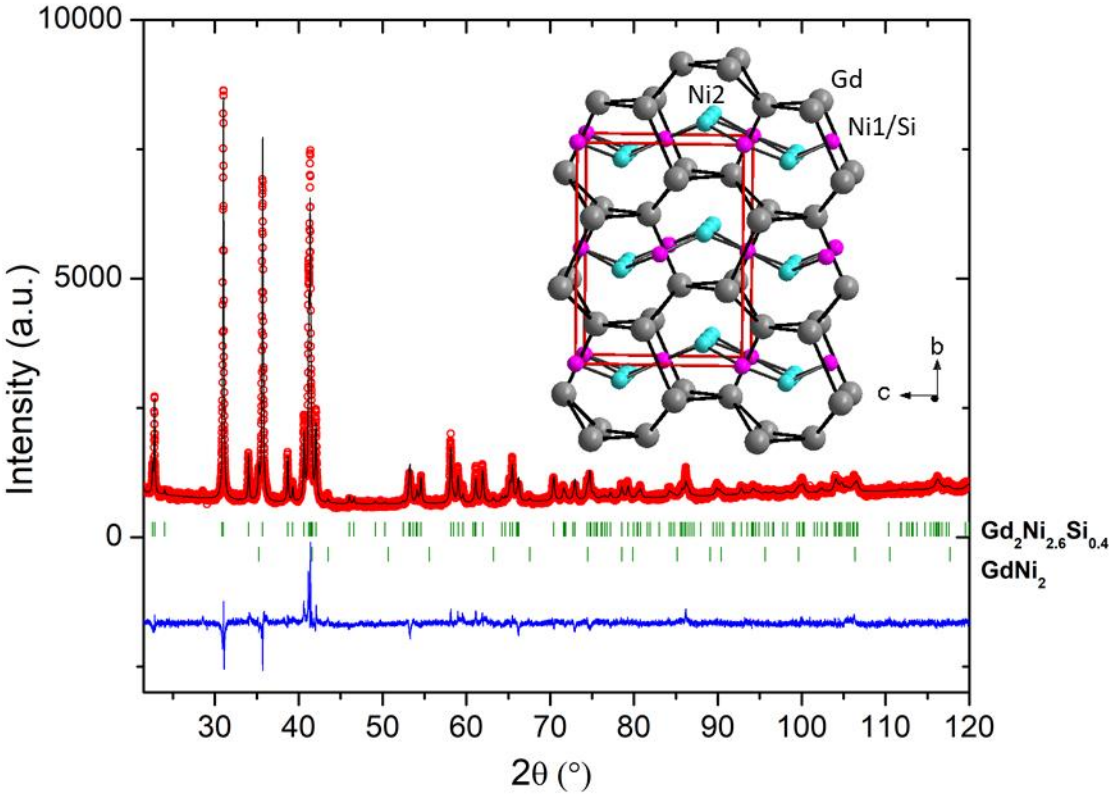

Figure 4. (Color online) Rietveld refinement of the crystal structure (inset) using the x-ray powder diffraction pattern of the as cast sample with nominal composition $Gd_{2.0}Ni_{2.6}Si_{0.4}$.

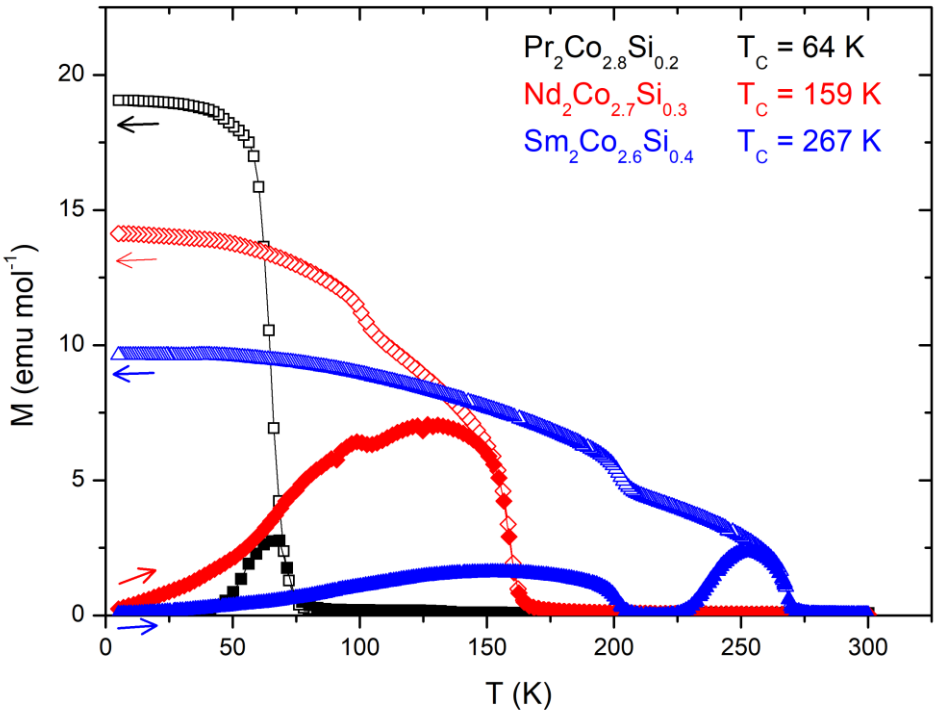

Figure 5. (Color online) Susceptibility versus temperature curves of the $R_2Co_{3-x}Si_X$ systems (*R* = Pr, Nd and Sm). The open and closed symbols correspond to field cooling (FC) and zero field cooling (ZFC) modes, respectively. The nominal compositions are displayed on the figure. The corresponding curve for *R* = Gd is described in reference [11].

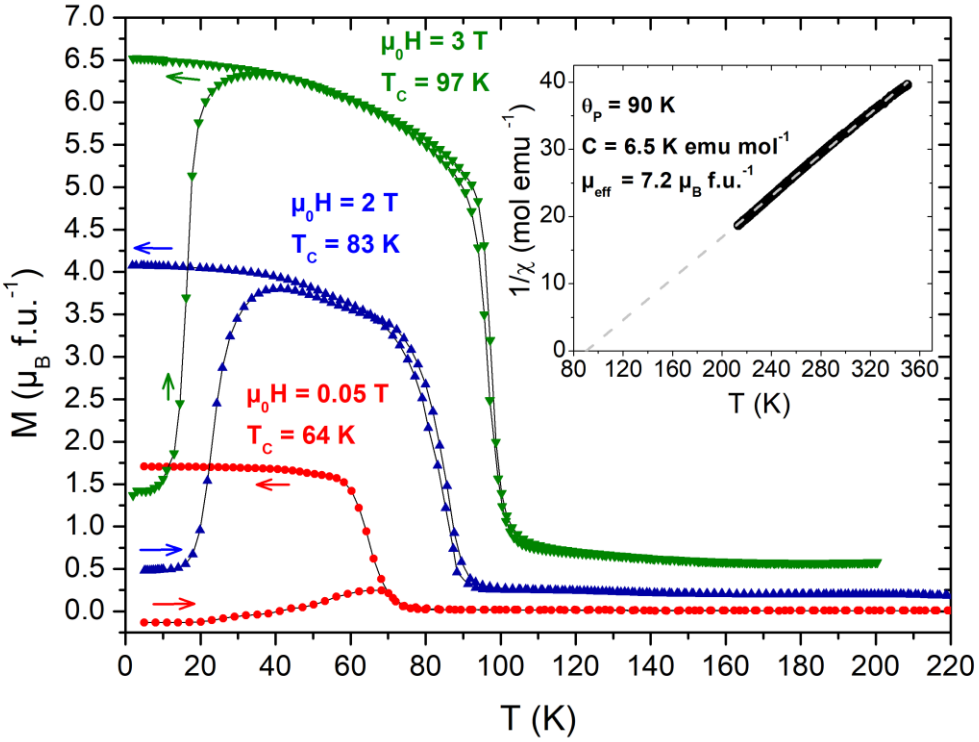

Figure 6. Zero-field cooled and field cooled magnetization of the $Pr_2Co_{2.8}Si_{0.2}$ system at 0.05, 2 and 3 T. Inset shows the inverse susceptibility at high temperatures plotted against temperature in a field of 2 T fitted using the Curie Weiss law.

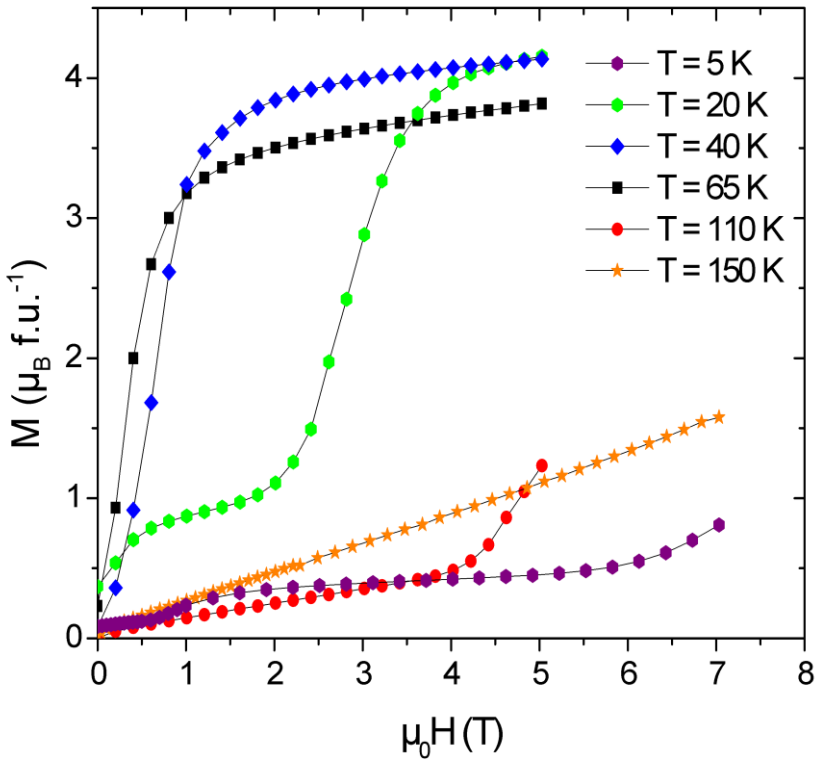

Figure 7. (Color online) Isothermal magnetization virgin curves of $Pr_2Co_{2.8}Si_{0.2}$ (Piece of sample).

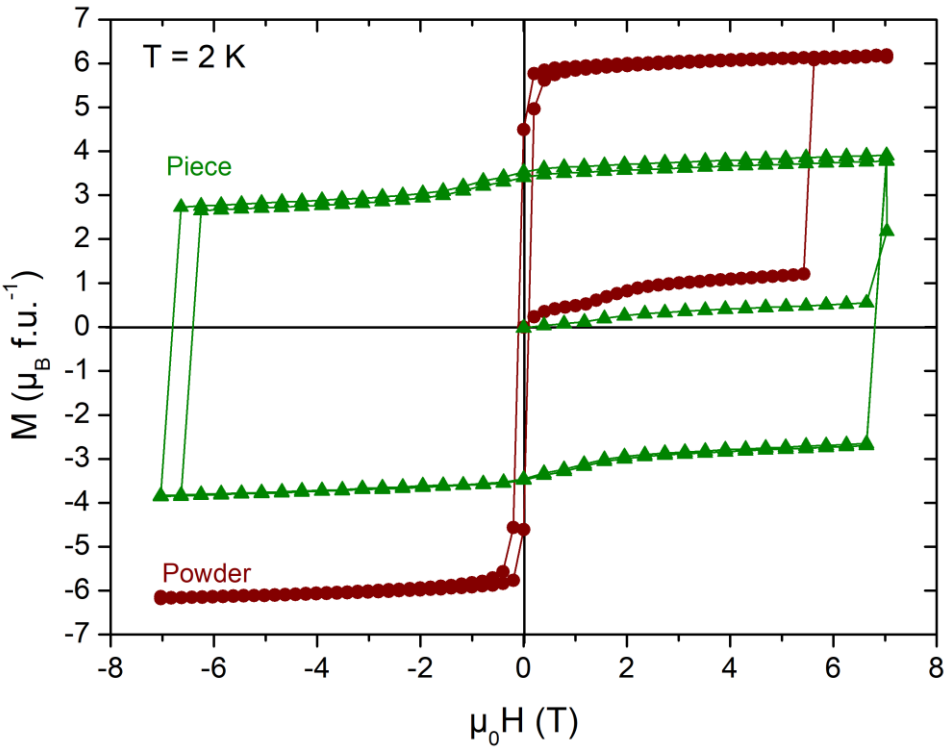

Figure 8. Magnetization hysteresis loops of $Pr_2Co_{2.8}Si_{0.2}$ measured at 2 K on a small piece and on powder (2 cycles).

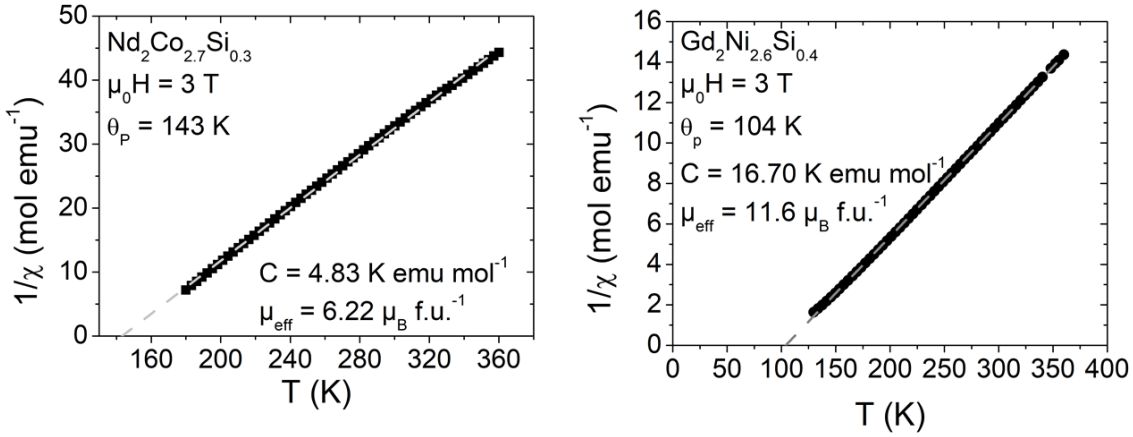

Figure 9. Plot of the inverse susceptibility of $Nd_2Co_{2.7}Si_{0.3}$ (left) and $Gd_2Ni_{2.6}Si_{0.4}$ (right) at high field fitted with the Curie-Weiss law

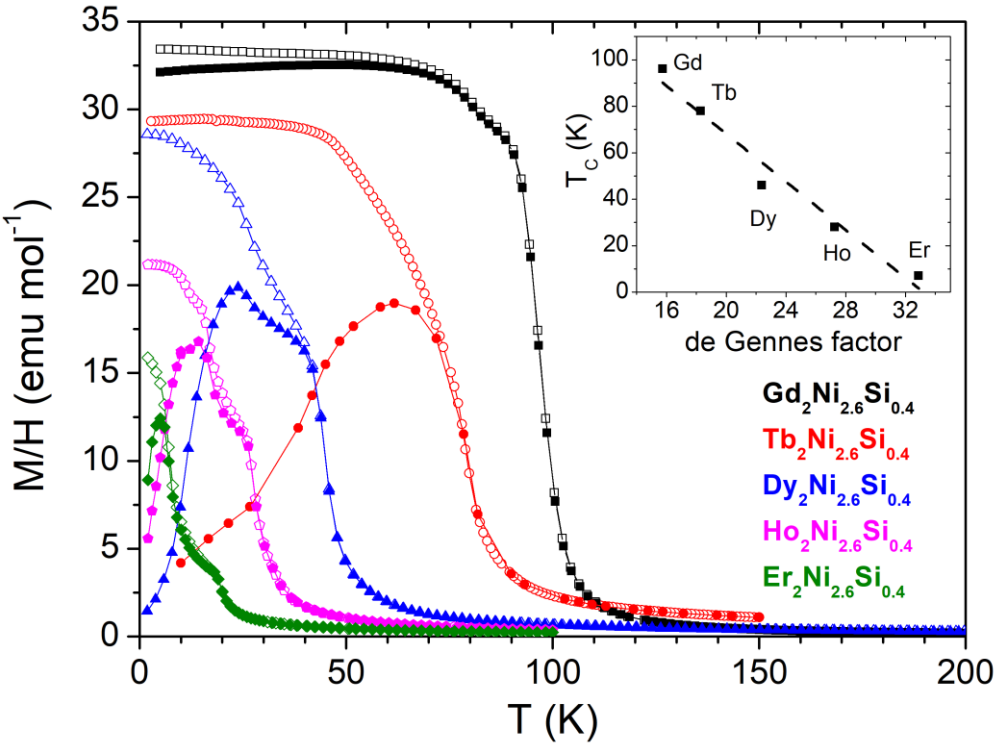

Figure 10. (Color online) Susceptibility versus temperature curves of the as cast $R_2Ni_{2.6}Si_{0.4}$ systems (R = Gd, Tb, Dy, Ho and Er) measured with μ_0H = 0.05 T. The open and closed symbols correspond to field cooling (FC) and zero field cooling (ZFC) modes, respectively. Inset shows a plot of the Curie temperatures for the $R_2Ni_{2.6}Si_{0.4}$ samples against the de Gennes factor for each of the trivalent rare earth elements.

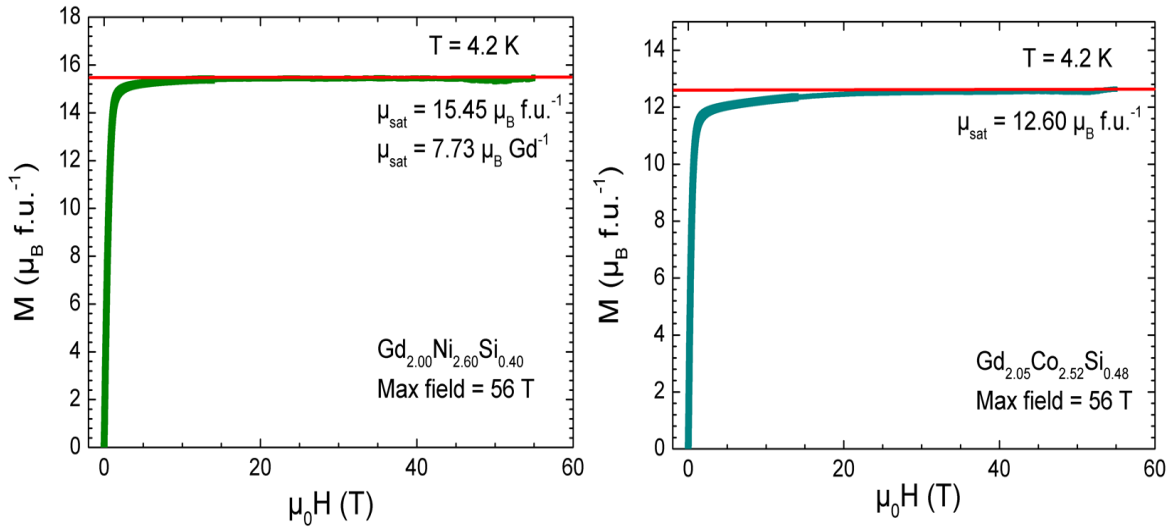

Figure 11. High field magnetization measurements for the samples with nominal composition $Gd_{2.00}Ni_{2.60}Si_{0.40}$ (left) and $Gd_{2.05}Co_{2.52}Si_{0.48}$ (right) up to 56 T. Both measurements were carried out at 4.2 K.

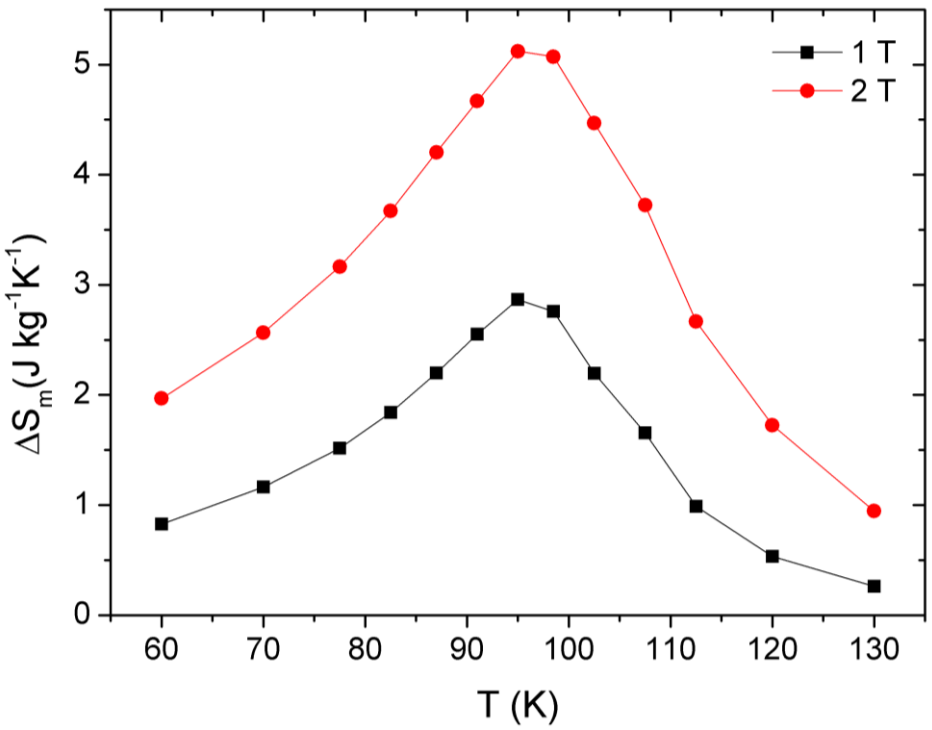

Figure 12. Temperature dependence of the magnetic entropy variation of $Gd_{2.00}Ni_{2.60}Si_{0.40}$ in a field of 1 T (black squares) and 2 T (red circles).

Acknowledgements

A portion of this work was performed at the Laboratoire National des Champs Magnétiques Intenses (LNCMI), which is supported by the European Magnetic Field Laboratory (EMFL).

References

[1] V.K. Pecharsky, K.A. Gschneidner Jr, Magnetocaloric effect in Gd5Si2Ge2/Gd composite materials, Phys. Rev. Lett. 78 (1997) 4494–4497. doi:10.1063/1.2158971.

[2] K.A. Gschneidner, V.K. Pecharsky, Thirty years of near room temperature magnetic cooling: Where we are today and future prospects, Int. J. Refrig. 31 (2008) 945–961. doi:10.1016/j.ijrefrig.2008.01.004.

[3] C. Vázquez-Vázquez, M. Lovelle, C. Mateo, M.A. López-Quintela, M.C. Buján-Núñez, D. Serantes, D. Baldomir, J. Rivas, Magnetocaloric effect and size-dependent study of the magnetic properties of cobalt ferrite nanoparticles prepared by solvothermal synthesis, Phys. Status Solidi. 205 (2008) 1358–1362. doi:10.1002/pssa.200778128.

[4] A.S. Chernyshov, A.O. Tsokol, A.M. Tishin, K.A. Gschneidner, V.K. Pecharsky, Magnetic and magnetocaloric properties and the magnetic phase diagram of single-crystal dysprosium, Phys. Rev. B. 71 (2005) 184410. doi:10.1103/PhysRevB.71.184410.

[5] K.A. Gschneidner Jr, V.K. Pecharsky, A.O. Tsokol, Recent developments in magnetocaloric materials, Reports Prog. Phys. 68 (2005) 1479–1539. doi:10.1088/0034-4885/68/6/R04.

[6] Q. Ji, B. Gao, G. Mu, T. Hu, W. Li, Y. Liu, Y. Ma, X. Xie, Enhancement of superconductivity by Sb-doping in the hole-doped iron-pnictide superconductor Pr1-xSrxFeAsO, Phys. C Supercond. Its Appl. 498 (2014) 50–53. doi:10.1016/j.physc.2014.01.002.

[7] M.C. Silva-Santana, C.A. Dasilva, P. Barrozo, E.J.R. Plaza, L. De Los Santos Valladares, N.O.

Moreno, Magnetocaloric and magnetic properties of SmFe0.5Mn0.5O3 complex perovskite, J. Magn. Magn. Mater. 401 (2016) 612–617. doi:10.1016/j.jmmm.2015.10.076.

[8] O. Gutfleisch, M.A. Willard, E. Brück, C.H. Chen, S.G. Sankar, J.P. Liu, Magnetic Materials and Devices for the 21st Century: Stronger, Lighter, and More Energy Efficient, Adv. Mater. 23 (2011) 821–842. doi:10.1002/adma.201002180.

[9] V. Franco, J.S. Blázquez, B. Ingale, A. Conde, The Magnetocaloric Effect and Magnetic Refrigeration Near Room Temperature: Materials and Models, Annu. Rev. Mater. Res. 42 (2012) 305–342. doi:10.1146/annurev-matsci-062910-100356.

[10] J. Lyubina, Magnetocaloric materials for energy efficient cooling, J. Phys. D. Appl. Phys. 50 (2017) 53002. doi:10.1088/1361-6463/50/5/053002.

[11] S. Tencé, R.C. Flores, J. Chable, S. Gorsse, B. Chevalier, E. Gaudin, Stabilization by Si substitution of the pseudobinary compound Gd 2(Co3-xSix) with magnetocaloric properties around room temperature, Inorg. Chem. 53 (2014) 6728–6736. doi:10.1021/ic500529b.

[12] C. Mayer, E. Gaudin, S. Gorsse, B. Chevalier, The new ternary silicide Gd5CoSi2: Structural, magnetic and magnetocaloric properties, J. Solid State Chem. 184 (2011) 325–330. doi:10.1016/j.jssc.2010.11.023.

[13] E. Gaudin, S. Tencé, F. Weill, J. Rodriguez Fernandez, B. Chevalier, Structural and Magnetocaloric Properties of the New Ternary Silicides Gd 6 M 5/3 Si 3 with M = Co and Ni, Chem. Mater. 20 (2008) 2972–2979. doi:10.1021/cm8000859.

[14] E. Gaudin, C. Mayer, F. Weill, B. Chevalier, Structural and magnetic properties of the new ternary silicide Gd3Co2.48 Si1.52, J. Alloys Compd. 545 (2012) 148–152. doi:10.1016/j.jallcom.2012.07.140.

[15] E. Gaudin, F. Weill, B. Chevalier, Structural, Magnetic and Electrical Properties of the Ternary Silicide Gd6Co1.67Si3 Derived from the hexagonal Ho4Co3.07(or Ho6Co4.61) type structure, Zeitschrift Fur Naturforsch. 61B (2006) 825–832.

[16] A. V. Morozkin, O. Isnard, R. Nirmala, S.K. Malik, Mo2NiB2-type {Gd, Tb, Dy)2Ni2.35Si0.65 and La2Ni3-type {Dy, Ho}2Ni2.5Si0.5 compounds: Crystal structure and magnetic properties, J. Solid State Chem. 225 (2015) 368–377. doi:10.1016/j.jssc.2015.01.017.

[17] J. Rodriguez-Carvajal, Recent Advances in Magnetic Structure Determination by neturon powder diffraction, Phys. B. 192 (1993) 55–69.

[18] J.H.N. Van Vucht, K.H.J. Buschow, The Crystal Structure of La2Ni3, J. Less Common Met. 46 (1976) 133–138.

[19] B.J. Beaudry, P.E. Palmer, The lattice parameters of La, Ce, Pr, Nd, Sm, Eu and Yb, J. Less Common Met. 34 (1974) 225–231. doi:10.1016/0022-5088(74)90163-5.

[20] R. Welter, G. Venturini, E. Ressouche, B. Malaman, Magnetic properties of RCoSi (R = La-Sm, Gd, Tb) compounds from susceptibility measurements and neutron diffraction studies, J. Alloys Compd. 210 (1994) 279–286. doi:16/0925-8388(94)90150-3.

[21] a. Szytuła, M. Bałanda, M. Hofmann, J. Leciejewicz, M. Kolenda, B. Penc, a. Zygmunt, Antiferromagnetic properties of ternary silicides RNiSi (R=Tb–Er), J. Magn. Magn. Mater. 191 (1999) 122–132. doi:10.1016/S0304-8853(98)00330-8.

[22] Y.G. Xiao, Q. Huang, Z.W. Ouyang, J.W. Lynn, J.K. Liang, G.H. Rao, Crystal and magnetic structures of Laves phase compound NdCo2 in the temperature range between 9 and 300 K, J.

Alloys Compd. 420 (2006) 29–33. doi:10.1016/j.jallcom.2005.10.073.

[23] W.A.J.J. Velge, K.H.J. Buschow, Magnetic and crystallographic properties of some rare earth cobalt compounds with CaZn5 structure, J. Appl. Phys. 39 (1968) 1717–1720. doi:10.1063/1.1656420.

[24] J.P. Liu, J.H.V.J. Brabers, A.J.M. Winkelman, A.A. Menovsky, F.R. de Boer, K.H.J. Buschow, Synthesis and magnetic properties of R2Co17Nx type interstitial compounds, J. Alloys Compd. 200 (1993) L3–L6. doi:10.1016/0925-8388(93)90461-U.

[25] B. Cordero, V. Gómez, A.E. Platero-Prats, M. Revés, J. Echeverría, E. Cremades, F. Barragán, S. Alvarez, Covalent radii revisited, Dalt. Trans. (2008) 2832. doi:10.1039/b801115j.

[26] F.H. Spedding, A.H. Daane, K.W. Herrmann, The crystal structures and lattice parameters of high-purity scandium, yttrium and the rare earth metals, Acta Crystallogr. 9 (1956) 559–563. doi:10.1107/S0365110X5600156X.

[27] A. V. Morozkin, A. V. Knotko, V.O.O. Yapaskurt, P. Manfrinetti, M. Pani, A. Provino, R. Nirmala, S. Quezado, S.K.K. Malik, The isothermal section of Gd-Ni-Si system at 1070 K, J. Solid State Chem. 235 (2016) 58–67. doi:10.1016/j.jssc.2015.12.019.

[28] L.J. de Jongh, J. Bartolomé, F.J.A.M. Greidanus, H.J.M. de Groot, H.L. Stipdonk, K.H.J. Buschow, Magnetic properties of PrCo2 and its Ternary Hydride PrCo2H4, J. Magn. Magn. Mater. 25 (1981) 207–214.

[29] K. Kanematsu, T. Sugiyama, M. Sekine, T. Okagaki, K.I. Kobayashi, Formation and magnetic properties of crystalline and amorphous SmCo2 hydrides, J. Less Common Met. 147 (1989) 9–18. doi:10.1016/0022-5088(89)90143-4.

[30] E. Burzo, R. Lemaire, On the Magnetic Behaviour of RCo2 compounds where R is Yttrium or a rare-earth, Solid State Commun. 84 (1992) 1145–1148.

[31] D. Gignoux, R. Lemaire, R. Mendia-Monterroso, J.M. Moreau, J. Schweizer, Antiferromagnetism in the La-Co system, Phys. B+C. 130 (1985) 376–378. doi:10.1016/0378-4363(85)90261-X.

[32] S.C. Abraham, J.L. Bernstein, R.C. Sherwood, J.H. Wbrnick, The crystal structure and magnetic properties of the rare-earth compounds nickel (RNi), J. Phys. Chem. Solids. 25 (1964) 1069–1080.

[33] S. Tencé, B. Chevalier, Magnetic and magnetocaloric properties of Gd2In0.8X0.2 compounds (X=Al, Ga, Sn, Pb), J. Magn. Magn. Mater. 399 (2016) 46–50. doi:10.1016/j.jmmm.2015.09.058.

[34] B. Stalinski, S. Pokrzywnicki, Magnetic Properties of Gd-Al intermetallic compounds, Phys. Solid State. 14 (1966) 57–60.

[35] A. Bajorek, G. Chełkowska, B. Andrzejewski, Magnetic properties, crystal and electronic structure of GdNi5-xCux series, J. Alloys Compd. 509 (2011) 578–584. doi:10.1016/j.jallcom.2010.09.195.

[36] S. Tencé, E. Gaudin, B. Chevalier, Around the composition Gd4Co3: Structural, magnetic and magnetocaloric properties of Gd6Co4.85(2), Intermetallics. 18 (2010) 1216–1221. doi:10.1016/j.intermet.2010.03.016.

[37] N.N. (Norman N. Greenwood, A. (Alan) Earnshaw, Chemistry of the elements, Butterworth-Heinemann Ltd. (1995) 1423–1449. doi:10.1016/S0277-5387(00)84180-7.